Perez, J., Freeman, H., Schuessler, J. A., Benning, L. G. (2019): The interfacial reactivity of arsenic species with green rust sulfate (GRSO4). - Science of the Total Environment, 648, 1161-1170.

https://doi.org/10.1016/j.scitotenv.2018.08.163

The interfacial reactivity of arsenic species with green rust sulfate (GR_{SO4})

Jeffrey Paulo H. Perez[a,b,*], Helen M. Freeman[a], Jan A. Schuessler[a,†], Liane G. Benning[a,b]

[a] GFZ German Research Center for Geosciences, Telegrafenberg, 14473 Potsdam, Germany

[b] Department of Earth Sciences, Free University of Berlin, 12249 Berlin, Germany

* Corresponding author: jpperez@gfz-potsdam.de

[†] Current address: Thermo Fisher Scientific GmbH, 28199 Bremen, Germany

Abstract

Arsenic (As) contamination in groundwater is a significant health and environmental concern worldwide because of its wide distribution and toxicity. The fate and mobility of As is greatly influenced by its interaction with redox-active mineral phases, among which green rust (GR), an Fe^{II}-Fe^{III} layered double hydroxide mineral, plays a crucial role. However, the controlling parameters of As uptake by GR are not yet fully understood. To fill this gap, we determined the interfacial reactions between GR sulfate (GR_{SO4}) and aqueous inorganic As(III) and As(V) through batch adsorption experiments, under environmentally-relevant groundwater conditions. Our data showed that, under anoxic conditions, GR_{SO4} is a stable and effective mineral adsorbent for the removal of As(III) and As(V). At an initial concentration of 10 mg L^{-1}, As(III) removal was higher at alkaline pH conditions (~ 95% removal at pH 9) while As(V) was more efficiently removed at near-neutral conditions (> 99% at pH 7). The calculated maximum As adsorption capacities on GR_{SO4} were 160 mg g^{-1} (pH 8-9) for As(III) and 105 mg g^{-1} (pH 7) for As(V). The presence of other common groundwater ions such as Mg^{2+} and PO_4^{3-} reduces the efficiency of As removal, especially at high ionic strengths. Long-term batch adsorption experiments (up to 90 days) revealed that As-interacted GR_{SO4} remained stable, with no mineral transformation or release of adsorbed As species. Overall, our work shows that GR_{SO4} is one of the most effective As adsorbents among iron (oxyhydr)oxide phases.

Keywords: arsenic; adsorption; green rust; groundwater treatment; iron (oxyhydr)oxide; layered double hydroxide

1. Introduction

Elevated levels of dissolved arsenic (As) in ground- and drinking waters remain a significant global environmental and public health concern because of the wide-spread occurrence and distribution, as well as toxicity and mobility of As in the environment (Vaughan, 2006). In groundwaters, As is commonly present as inorganic oxyanions arsenite ($H_3As^{III}O_3$) and arsenate ($H_3As^{V}O_4$), with the former being the more toxic form (Hughes, 2002; Sharma and Sohn, 2009). Based on their acid dissociation constants, As(III) forms the neutral species $H_3As^{III}O_3$ at moderately reducing conditions ($pK_{a1,2,3}$ = 9.23, 12.13, 13.40) while As(V) is present as $H_2As^{V}O_4^-$ and $HAs^{V}O_4^{2-}$ ($pK_{a1,2,3}$ = 2.20, 6.97, 11.53) in oxidized environments (Ferguson and Gavis, 1972; Inskeep et al., 2002). However, it is important to note that the relatively slow redox transformation kinetics allows both As(III) and As(V) to persist under both anoxic and oxic conditions (Masscheleyn et al., 1991).

Green rust (GR) minerals are redox-active phases, which belong to the family of Fe^{II}-Fe^{III} layered-double hydroxides (LDHs). Their ability to treat or remove toxic metals from groundwater has been investigated (Usman et al., 2018), yet the fundamental adsorption properties or uptake capacities of metals on GR phases have still not been quantified. The high potential of GR as a material for groundwater remediation stems from its structural and redox properties. GR is composed of positively charged brucite-like layers of octahedrally coordinated Fe^{II}-Fe^{III} hydroxides that alternate with negatively charged interlayers of anions and water molecules, as well as monovalent cations (Christiansen et al., 2009). These brucite-like layers and interlayer regions are held together by hydrogen bonding and electrostatic forces. GR is typically represented by the general formula, $[Fe^{II}_{(1-x)}Fe^{III}_x(OH)_2]^{x+}[(x/n)\ A^{n-}\cdot mH_2O]^{x-}$, where A^{n-} is the intercalated anion such as Cl^-, CO_3^{2-} and SO_4^{2-}, and x is the molar fraction of Fe^{III}, $[Fe^{III}]/[Fe_{total}]$ (Géhin et al., 2002). These properties allow GR to remove toxic metal contaminants by adsorption (Jönsson and Sherman, 2008; Mitsunobu et al., 2009), reduction (Christiansen et al., 2011; O'Loughlin et al., 2003; Skovbjerg et al., 2006), interlayer intercalation (Refait et al., 2000), and substitution of structural Fe in the octahedral sheets (Ahmed et al., 2008; Refait et al., 1990).

Considering the worldwide health implications of As-contaminated ground- and drinking waters (World Health Organization, 2017), it is paramount that we understand the removal efficiency

of As through interactions with various mineral substrates. There is an imminent challenge regarding the development, testing and validating the usefulness of adequate mineral phases that have high metal-specific uptake capacities, strong binding affinities and excellent stabilities. Adsorption-based technologies are promising groundwater clean-up strategies because of their facile implementation, relative cost-effectiveness and high removal efficiency (Leus et al., 2017). However, to optimize the efficiency of subsurface remediation strategies, the interactions between inorganic As species and the surfaces of redox-active minerals such as GR must be quantified in detail.

Su and Wilkin (2005) examined the interaction of As(III) and As(V) with synthetic green rust carbonate (GR_{CO3}) and monitored the changes in the aqueous phase. Their results showed that As(V) removal rates using GR_{CO3} were higher compared to As(III) due to the higher affinity of iron (oxyhydr)oxides for As(V) than the more toxic As(III). The mechanism of adsorption of As species onto GR mineral phases (e.g., GR_{Cl}, GR_{CO3}, GR_{SO4}) has also been investigated previously using X-ray absorption spectroscopy (XAS) (Jönsson and Sherman, 2008; Randall et al., 2001; Wang et al., 2010). In these studies, As(III) and As(V) were found to both form bidentate binuclear (^2C) and monodentate mononuclear (^1V) inner-sphere complexes on the FeO_6 octahedra at the edges of the GR crystal. However, the fundamental adsorption parameters (e.g., effects of pH, adsorbent loading, ionic strength, potentially competing ions), as well as the maximum uptake capacity and critical adsorption kinetics, necessary for understanding interactions between GR and As in groundwaters have never been evaluated in detail.

Herein, we aim to close this gap through an in-depth investigation on the interfacial interactions between freshly-precipitated green rust sulfate (GR_{SO4}) and aqueous inorganic As species. We evaluated the performance of GR_{SO4} as an effective adsorbent for the removal of arsenite [As(III)] and arsenate [As(V)] by examining adsorption reactions as a function of pH, adsorbent loading, ionic strength, varying initial As concentrations, time and the presence of potentially interfering ions in groundwater. Our results reveal that GR_{SO4} is a highly effective adsorbent for the removal of As species from groundwater.

2. Materials and methods

2.1 Mineral synthesis and characterization

GR with interlayer sulfate (GR_{SO4}) was synthesized in an anaerobic chamber (95% N_2, 5% H_2, Coy Laboratory Products, Inc.) at room temperature using the co-precipitation method (Géhin et al., 2002). In brief, separate Fe(II) (0.3 M) and Fe(III) (0.1 M) solutions were prepared from reagent grade $(NH_4)_2Fe(SO_4)_2 \cdot 6H_2O$ and $Fe_2(SO_4)_3$ salts (VWR) and deoxygenated Milli-Q water (~18.2 MΩ cm^{-1}). GR synthesis was initiated by mixing the Fe(III) and Fe(II) solutions (pH ~2) under constant stirring at 350 rpm. Subsequently, a 0.3 M NaOH solution was slowly titrated into the mixed Fe^{II}-Fe^{III} solution until the pH reached 8. Base addition resulted in the precipitation of a dark blue-green suspension, which was stirred and aged further for one hour. The suspension was then washed with O_2-free Milli-Q water to remove excess solutes. The yield of the washed GR_{SO4} slurry was determined based on the difference between the total Fe concentration of an aliquot of the suspension dissolved in 0.3 M HNO_3 and the dissolved Fe concentration in the supernatant after filtration through a 0.2-µm syringe filter. The Fe ion concentration was analyzed by inductively coupled plasma optical emission spectrometry (ICP-OES). Each batch of GR_{SO4} slurry (~8.2 g L^{-1}) was prepared fresh and kept in the anaerobic chamber adsorption experiments for a maximum of 24 h.

The solid GR_{SO4} samples were analyzed by X-ray powder diffraction (XRD), nitrogen sorption, transmission electron microscopy (TEM), selected area electron diffraction (SAED), energy dispersive X-ray spectroscopy (EDX), electron energy-loss spectroscopy (EELS), high angle annular dark field scanning transmission electron microscopy (HAADF-STEM), X-ray photoelectron spectroscopy (XPS) and Mössbauer spectroscopy to determine their structure, particle sizes, morphologies, surface properties, as well as redox and full chemical composition. Detailed information on all phase characterizations can be found in the Supporting Information (Text S1).

2.2 Adsorption experiments

All batch adsorption experiments were carried out in triplicate at room temperature inside the anaerobic chamber using headspace crimp vials with the washed GR_{SO4} suspensions (S/L = 4 g L^{-1}) reacted with 10 mg L^{-1} aqueous As(III) or As(V) solutions. The mixed samples were shaken at 250

rpm for 24 h followed by the separation of solids and supernatants by filtration through 0.22-µm syringe filters. The obtained liquid phases were acidified (pH ~2 with Merck Suprapur® grade HNO_3) and stored at 4°C until analysis. The elemental composition of the liquid phases was determined following the method described in Schuessler et al. (2016) using an axial ICP-OES Varian 720ES. Full details of all tested parameters [e.g., varying pH (7 to 9), adsorbent loading (solid to solution ratio, S/L 2 to 6 g L^{-1}), ionic strength (IS* 0.5 to 0.005 M), competing ions (Ca^{2+}, Mg^{2+}, PO_4^{3-}) and time (5 min to 90 days)] for the batch adsorption experiments and analytical methods can be found in the Supporting Information (Text S1, Table S1).

2.3 Adsorption kinetics and isotherms

Kinetic rates of As adsorption were determined at pH 8 using an initial As concentration of 10 mg L^{-1} and an adsorbent loading of 4 g L^{-1}. The mixtures were shaken for 5 min, 10 min, 15 min, 30 min, 1 h, 2 h, 4 h, 8 h, 16 h and 24 h after which the solids were separated from the supernatant and analysed as described above. Adsorption isotherms were obtained at room temperature and at pH 7 and 8-9 using an adsorbent loading of 4 g L^{-1}, initial As concentrations up to 1,000 mg L^{-1} and contact time of 24 h. The obtained equilibrium adsorption data were fitted to the Langmuir and Freundlich isotherm models (Limousin et al., 2007).

3. Results and discussion

3.1 Synthesis and characterization of GR_{SO4}

The morphology, size and chemical composition of the synthesized GR_{SO4} particles were characterized by TEM imaging and analytical spectroscopy. The micrographs (Fig. 1a) of the synthesized material revealed a well-defined hexagonal plate-like morphology typical of GR_{SO4} (Géhin et al., 2002). The diameter of particles varied between 50 and 500 nm while the estimated thickness of the particles calculated by the log-ratio (relative) method (Malis et al., 1988) from the low loss EEL spectra was around 16 to 20 nm. The SAED pattern (Fig. 1a inset) shows the distinctive hexagonal *c*-axis spot pattern of a single crystal GR_{SO4} (Ahmed et al., 2010). The elemental composition (Table S2), which was calculated from the EDX spectra, is comparable to the theoretical

values based on the chemical formula, $Fe^{II}_4Fe^{III}_2(OH)_{12}SO_4 \cdot 8H_2O$ (Simon et al., 2003). The mineralogy of the freshly-precipitated material was confirmed through XRD patterns (Fig. S1) to be pure GR_{SO4} as evidenced through the typical sharp and symmetric basal (00*l*) reflections corresponding to the interlayer distances between the Fe^{II}-Fe^{III} octahedral hydroxide sheets (Simon et al., 2003). No other iron (oxyhydr)oxide phases were identified in the freshly-precipitated GR_{SO4} samples.

The oxidation state of Fe can be determined by the EELS Fe L_3-edge position and shape, where octahedrally coordinated Fe(III) has a peak energy ~1.8 eV higher than octahedrally coordinated Fe(II) (Brown et al., 2017). Separate peaks attributed to Fe^{2+} (709 eV) and Fe^{3+} (710.8 eV) within the primary L_3 peak are resolvable when EEL spectra are acquired at higher resolution EELS (< 0.3 eV). Using the EELS resolution of the microscope used for this work (0.8 eV), the Fe(II)/Fe(III) ratio was estimated by comparing our experimental spectra to reference spectra collected under the same conditions. Theoretical spectra were calculated by stoichiometrically combining the intensity-normalized spectra of the Fe standards for hedenbergite (octahedrally coordinated Fe^{2+}) and hematite (octahedrally coordinated Fe^{3+}). This resulted in a theoretical spectrum for GR_{SO4} (where Fe(II)/Fe(III) = 2) which allowed for the direct comparison between the Fe L_3 peak shape and position in our sample and the theoretical spectrum (blue line in Fig.1b; Fig. S2a). This revealed that the shape of the Fe L_3-edge for the GR_{SO4} sample matched the linear reference fit for a Fe(II)/Fe(III) ratio of 2, with minor differences. This is evidenced by the changes in shape and position of the L_3 peak in the theoretical spectrum as the GR composition becomes more Fe(III)-rich. This is also clearly shown in Fig. S2, where the theoretical spectra for Fe(II)/Fe(III) ratios from 1 to 0.2, and the residual of each fit are shown. These results suggest that our sample had a Fe(II)/Fe(III) ratio corresponding to 2.

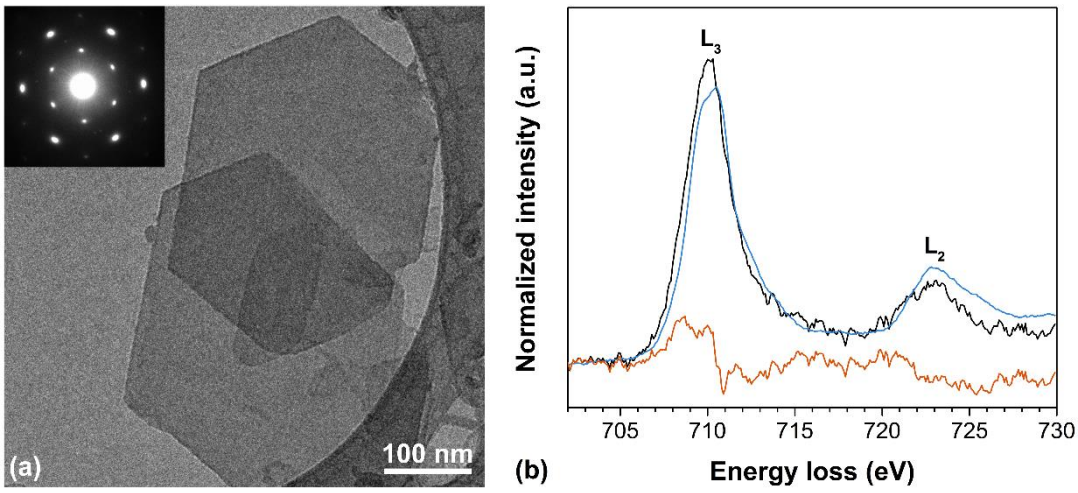

Fig. 1. (a) TEM image of GR_{SO4} with SAED pattern of a single particle in inset. (b) Fe $L_{2,3}$-edge EEL spectrum of GR_{SO4} sample (black), linear reference fit (blue) and residual spectrum (orange).

The surface chemistry of the synthesized GR_{SO4} was analyzed by XPS and the wide scan spectrum (Fig. S3) revealed photoelectron peaks of Fe *2p*, O *1s* and S *2p* at binding energies of 710.7, 531.9 and 168.8 eV, respectively. The Fe $2p_{1/2}$ and $2p_{2/3}$ photoelectron peaks (Fig. 2a) were observed at 724.0 and 710.7 eV, respectively. The value of the Fe $2p_{2/3}$ peak maxima was shifted to slightly higher binding energy compared to a GR with interlayer carbonate (GR_{CO3}, 709.4 eV), which also has an Fe(II)/Fe(III) ratio of 2.0 (Mullet et al., 2008). This indicates a slightly higher Fe(III) content in our synthesized GR_{SO4}. However, the presence of a characteristic Fe(II) satellite peak at 726.7 eV and a Fe(III) satellite peak at 731.0 eV confirmed the presence of both Fe(II) and Fe(III) in our sample at the desired ratio of 2. The peak shape and positions of the Fe $2p_{1/2}$ and $2p_{2/3}$ photoelectron peaks were also similar to previously reported XPS spectra for GR_{SO4} (Nedel et al., 2010). Furthermore, the relative contributions of the deconvoluted O *1s* peaks at 530.2, 531.8 and 532.6 eV (Fig. 2b) that were assigned to Fe-O, O-H and adsorbed water (Table S3), respectively, were in agreement with values obtained by Mullet et al. (2008). The S *2p* doublet (Fig. 2c) at 168.8 eV confirmed the presence of SO_4^{2-} in the interlayer region.

The iron chemistry of the synthesized GR_{SO4} was characterized by Mössbauer spectroscopy which revealed two apparent doublets (Fig. S3), but with a certain line broadening of the outer doublet and a slight asymmetry of its line shape. An improved fit shown in Fig. 2d was obtained by

using three doublets D_1, D_2 and D_3 (hyperfine parameters, see Table S4). In this fit, doublets D_1 and D_2 correspond to high spin Fe(II) cations in the brucite-like octahedral sheets while doublet D_3 corresponds to high spin Fe(III) cations (Géhin et al., 2002). The relative areas of the doublets in the Mössbauer spectrum allowed us to calculate an Fe(II)/Fe(III) ratio in the GR_{SO4} sample of 2.09, which is in agreement with the ratio of 2 from our EELS data (Fig. 1b, Fig S2), as well as literature data (Géhin et al., 2002; Simon et al., 2003). However, it should be noted that the Mössbauer spectra for GR_{SO4} reported in literature are usually fitted with one Fe(II) doublet (Fig. S3, Table S5) instead of two doublets (Fig. 2d). It is worth noting nevertheless, that in our GR_{SO4}, the two doublets D_1 and D_2 revealed the same isomer shift, but these differed somewhat in their quadrupole splittings (ΔE_Q), thereby suggesting the presence of two inequivalent Fe(II) sites. The component with the largest ΔE_Q was attributed to Fe(II) ions far away from the anions (Génin and Ruby, 2004), whereas the presence of a component with smaller ΔE_Q suggested the presence of Fe(II) sites containing anions in their environment. Such components have been previously observed in Mössbauer spectra of GR samples with other interlayer anions like carbonate or chloride but not for sulfate (Génin and Ruby, 2004).

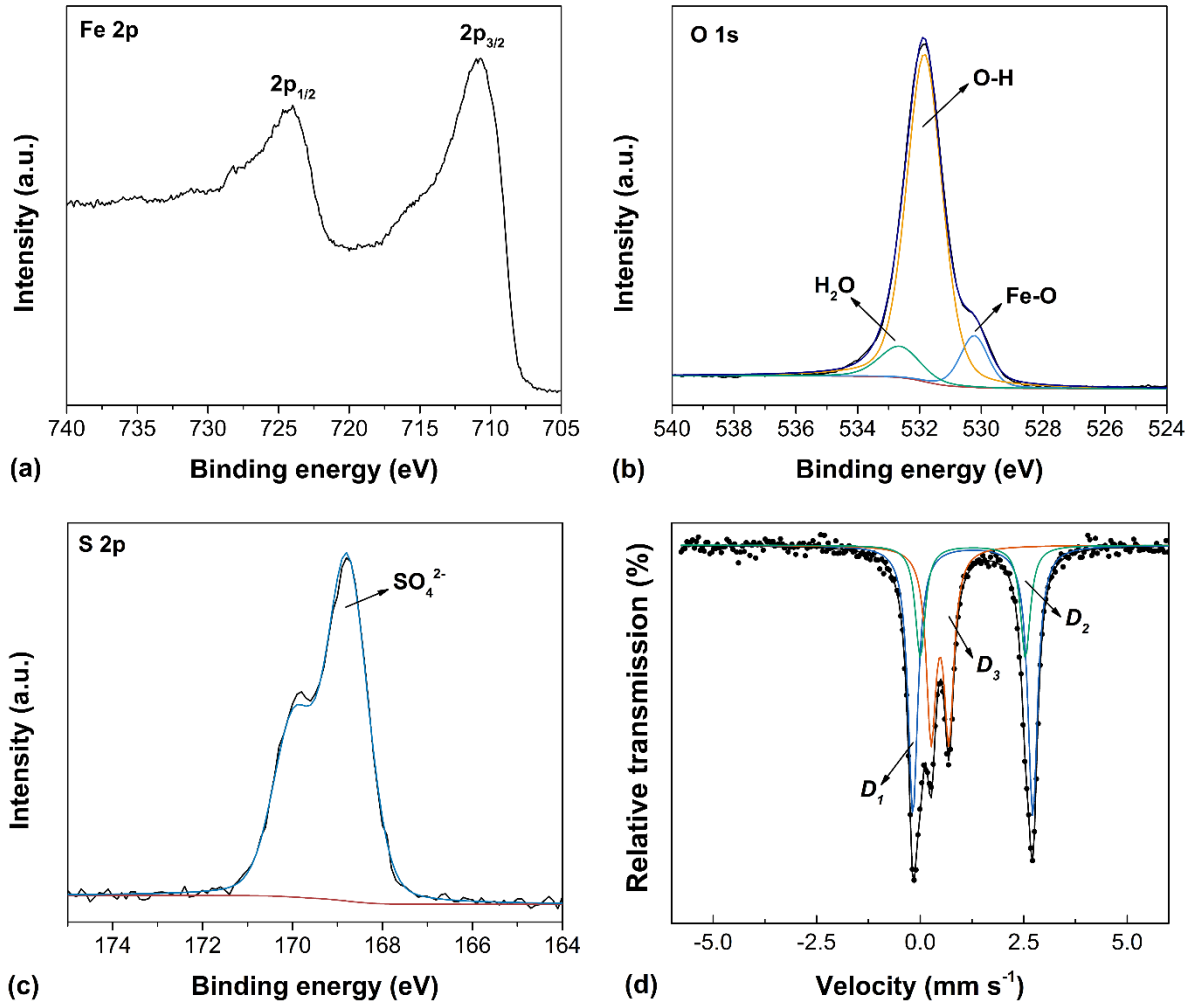

Fig. 2. (a-c) High resolution XPS spectra of GR_{SO4}: (a) Fe *2p*, (b) O *1s* and (c) S *2p* spectra. (d) ^{57}Fe Mössbauer spectrum of GR_{SO4} recorded at 20 K and fitted with three doublets.

3.2 Influence of environmental parameters on As removal

The effect of pH, adsorbent loading (solid to liquid ratio, S/L), ionic strength (IS*) and the presence of other potentially interfering aqueous groundwater ions were investigated to determine their influence on the adsorption of As species on GR_{SO4}. The removal efficiencies of GR_{SO4} for As(III) and As(V) at an initial concentration of 10 mg L^{-1} and under the above mentioned varying conditions are shown in Fig. 3.

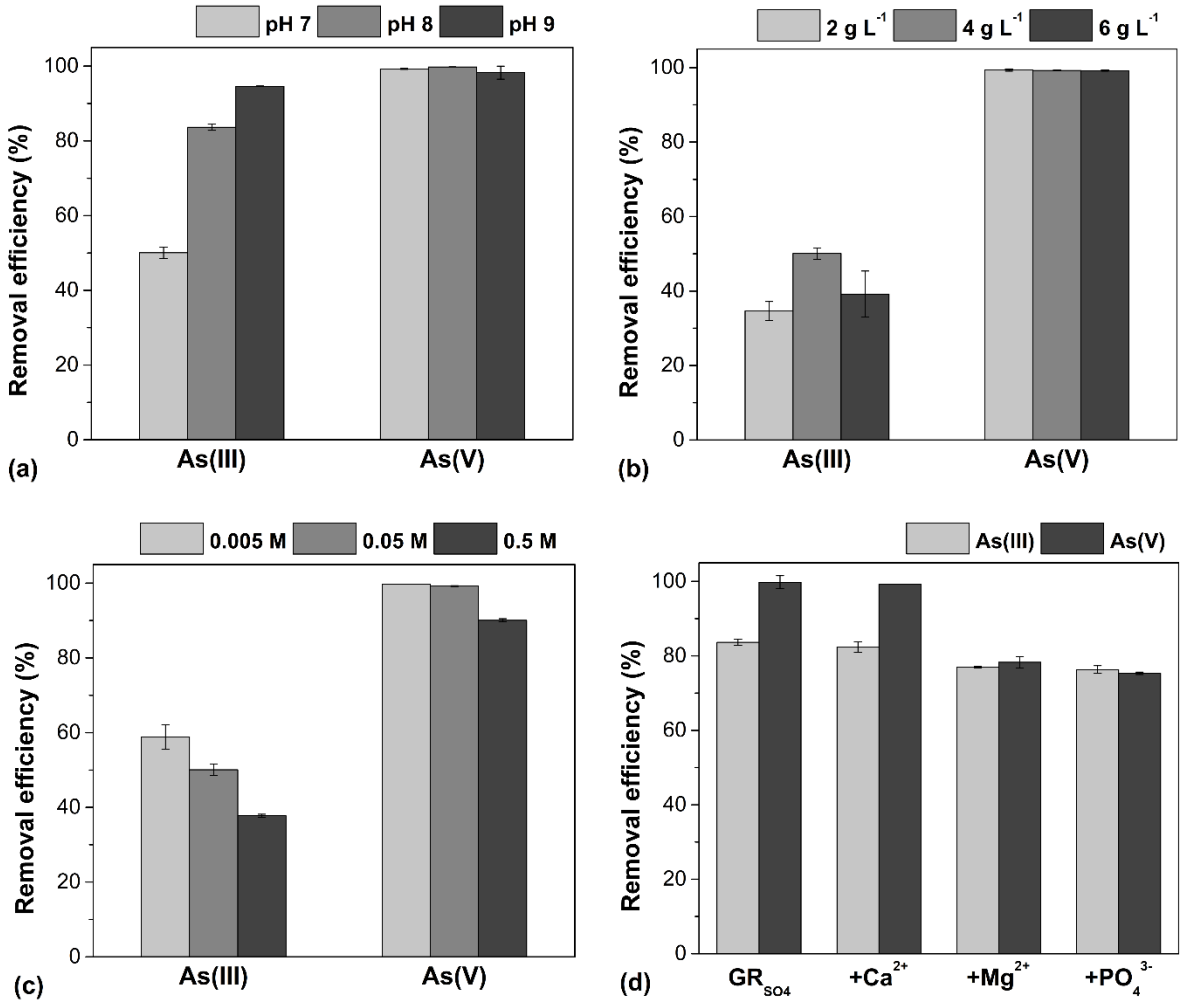

Fig. 3. Removal of 10 mg L^{-1} As(III) and As(V) upon interaction with GR_{SO4} after 24 h as a function of: (a) pH (S/L = 4 g L^{-1}, IS* = 0.05 M), (b) adsorbent loading, S/L (pH 7, IS* = 0.05 M), (c) ionic strength, IS* (pH 7, S/L = 4 g L^{-1}) and (d) presence of competing groundwater ions (at pH 8 and IS* = 0.05 M): pure GR_{SO4} (no competing ion), Ca^{2+} (100 mg L^{-1}), Mg^{2+} (50 mg L^{-1}) or PO_4^{3-} (10 mg L^{-1}). Error bars represent standard deviations of triplicate experiments (< 5% relative). Note: IS* here is defined as the ionic strength based on a 10x and 100x dilution from the initial 0.5 M IS of the GR_{SO4} suspension (further details, see in Supporting Information Text S1).

At all pH values tested, the As(V) removal efficiencies (Fig. 3a) were higher compared to As(III). This is likely because of the higher adsorption affinity of the pentavalent species on iron (oxyhydro)oxide surfaces. No significant differences in As(V) removal efficiencies between pH 7, 8 and 9 were observed (i.e. within analytical uncertainties < 2%). Although there were no significant

differences in removal efficiencies, GR_{SO4} can effectively remove As(V) at a relatively wide range of pH conditions that can be found in contaminated groundwaters (Nickson et al., 2000; Smedley and Kinniburgh, 2002; Zahid et al., 2008). In contrary, the removal efficiency of As(III) by GR_{SO4} was significantly affected by pH, which is the opposite of what was expected. With pH, As(III) removal efficiency (50.1 ± 1.5% at pH 7) increased by more than 30% at pH 8 (83.7 ± 0.9%) and another 10% increase was measured at pH 9 (94.6 ± 0.1%). Such surface polymerization of As(III) complexes has been previously suggested for GR_{Cl} and GR_{CO3} by XAS analysis (Ona-Nguema et al., 2009; Wang et al., 2010). Usually, the influence of pH on As adsorption by iron (oxy)hydroxides is controlled by two factors: (1) the speciation of the As in solution and (2) the point of zero charge (PZC) of the adsorbent. Over the pH range tested here, As(III) will mostly exist as $H_3AsO_3^0$ and $H_2AsO_3^-$ species while As(V) is present as $H_2AsO_4^-$ and $HAsO_4^{2-}$ species (Jain et al., 1999). For GR_{SO4} with a PZC of 8.3 (Guilbaud et al., 2013), the net surface charges will be negative at pH > 8.3 and positive at pH < 8.3. As a result of electrostatic repulsion caused by similar negative charges, one would expect the removal of both As(III) and As(V) species to decrease as the pH is increased from 8 to 9, which was not observed in our study. Particularly, for As(III), the biggest increase in removal was observed between pH 7 and 8 with a lesser change between 8 and 9 (Fig. 3a.). Similar trends have been observed for As interacted with GR_{CO3} (Jönsson and Sherman, 2008) and ferrihydrite (Jain et al., 1999; Raven et al., 1998). An increased As(III) adsorption at higher pH can be attributed to the possible formation of multi-nuclear complexes on the surfaces of GR_{SO4}.

With increased adsorbent loading from 2 to 4 g L^{-1}, the removal efficiency of As(III) also increased by ~15% from 34.6 ± 2.7 to 50.1 ± 1.5% (Fig. 3b). This increase was caused by the larger number of active surface sites available for As(III) complexes (Asere et al., 2017). However, with further increase in loading to 6 g L^{-1}, the efficiency decreased to 39.2 ± 6.2%. In the case of As(V), no significant differences (< 0.3% relative) in removal efficiencies were observed among the adsorbent loadings tested (Fig. 3b).

The removal efficiencies for both As species decreased with increasing ionic strength, IS* (Fig. 3c). For As(V), this decrease was only about 10% (from > 99.8 to 90.1 ± 0.4%) as ionic strength increased from 0.005 to 0.5 M. On the other hand, this inhibitory effect was more pronounced for

As(III) where the removal efficiency decreased 58.9 ± 3.2% at an ionic strength of 0.005 M to 37.8 ± 0.4% at an ionic strength of 0.5 M, although the overall removal was lower compared to As(V). The decrease in As removal at higher IS* can be caused by the decrease in available surface sites of GR_{SO4}. This results from potential aggregation of GR_{SO4} particles due to disturbances in the electrostatic double layer (Shipley et al., 2009). Although the presence of ionic species in the supernatant can also decrease the removal efficiency, the dissolved solutes in our experiments (e.g., Fe^{2+}, NH_4^+, Na^+, Cl^- and SO_4^{2-} ions) have been shown to have little or no effect on As adsorption (Asere et al., 2017; Guo and Chen, 2005; Gupta et al., 2009).

Common aqueous groundwater ions can compete for the available active surface sites on GR_{SO4} (Folens et al., 2016; Leus et al., 2018). We tested the effect of relevant dissolved potentially interfering ions in the water matrix through competitive adsorption experiments with Ca^{2+} (100 mg L^{-1}), Mg^{2+} (50 mg L^{-1}) or PO_4^{3-} (10 mg L^{-1}) and As (10 mg L^{-1}) to the GR_{SO4} suspension at pH 8. The concentrations of the competing ions were chosen based on the average aqueous ion concentrations in As-contaminated groundwaters in Bangladesh and West Bengal, India (Nickson et al., 2000; Zahid et al., 2008) and mining-contaminated groundwater sites (Smedley and Kinniburgh, 2002; Williams et al., 1996). The comparison (Fig. 3d) revealed no significant change in the removal of As(III) and As(V) resulting from the presence of Ca^{2+} ions. On the other hand, the presence of Mg^{2+} ions decreased the removal efficiency by 6.7 ± 1.0% for As(III) and 21.5 ± 2.1% As(V) compared to the Mg^{2+} free system. However, analysis of the liquid phases by ICP-OES revealed that Mg^{2+} was not adsorbed on GR_{SO4}, but remained solvated in the supernatant. This decrease in As removal can be caused by the high ionic potential of Mg^{2+}, allowing it be solvated by water molecules (Lightstone et al., 2001) and resulting in the formation outer-sphere hydrated Mg^{2+} complexes. Such aqueous complexes could potentially reduce the accessibility of active surface sites of GR_{SO4} for As adsorption. The presence of PO_4^{3-} ions also resulted in the inhibition of As adsorption, where the removal efficiency for As(III) and As(V) decreased by 7.3 ± 1.3 and 24.5 ± 1.8%, respectively. Phosphate, with a tetrahedral molecular geometry analogous to the structure of AsO_4^{3-}, can also form complexes in the same lateral (010) and (100) GR surfaces sites where As complexes bind (Bocher et al., 2004). This can result in a competition between PO_4^{3-} and As species on the available GR_{SO4}

284 binding sites, thereby explaining the reduced As removal efficiency. Remarkably, the phosphate
285 removal efficiency was > 90% for both the As(III) and As(V) competitive adsorption experiments.
286 This likely results from the higher affinity of iron (oxyhydr)oxides for phosphate compared to As, as
287 indicated by its higher sorption equilibrium constant (Roberts et al., 2004), and the slow exchange of
288 initially adsorbed phosphate on the GR_{SO4} surface sites with the competing As species (Hongshao and
289 Stanforth, 2001).
290
291 *3.3 Adsorption kinetics*
292 The rate of As removal over 24 h was determined at pH 8 by measuring the adsorption
293 kinetics in batch experiments at initial As concentration of 10 mg L^{-1} As(III) or As(V), S/L of 4 g L^{-1}
294 and an ionic strength of 0.05 M. After fitting the kinetic data with various adsorption models, the best
295 fit (R^2 > 0.9999) resulted from the pseudo-2nd order kinetic model (Ho, 2006). The linearized plots for
296 the pseudo-2nd order kinetic model are shown in Fig. 4. The calculated adsorption rate constants (k_2;
297 Table S6) revealed that the uptake of both As species was very fast. Full adsorption (> 99% removal)
298 of As(V) was achieved within 30 min of contact with $GR_{SO4,}$ while As(III) reached equilibrium after 4
299 h. The more rapid removal of As(V) was caused by the stronger binding affinity of pentavalent over
300 the trivalent As species to iron (oxyhydr)oxides (Roberts et al., 2004). These fast adsorption uptake
301 rates show that GR_{SO4} can efficiently remove As(III) and As(V) within a short time.
302
303

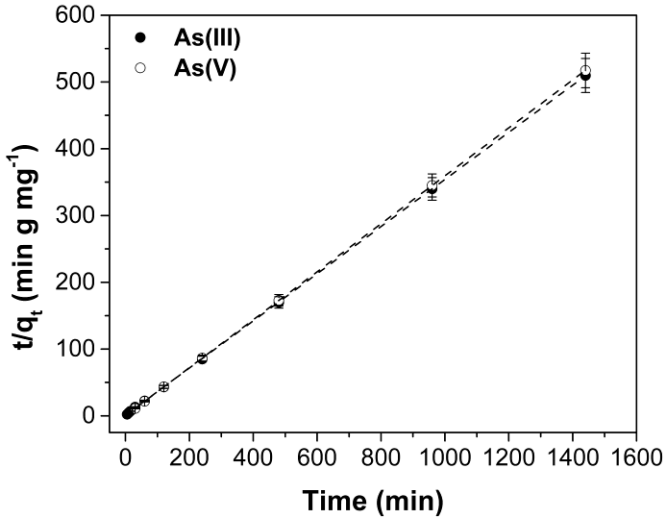

Fig. 4. Pseudo-2nd order kinetic data and model fits for the adsorption of As species on GR_{SO4}. Initial concentration is 10 mg L^{-1} at pH 8, S/L ratio of 4 g L^{-1} and IS* of 0.05 M. Error bars represent analytical uncertainty (< 5% relative) based on replicate measurements of QC solutions analyzed together with the samples (Table S1).

3.4 Long-term batch adsorption experiments

At an initial As concentration of 10 mg L^{-1}, GR_{SO4} remained stable during the course of the 90-day monitoring of batch adsorption experiments. No other iron (oxyhydr)oxide mineral phases were identified in XRD patterns of these long-term equilibrated and As-interacted samples (Fig. 5a). The TEM images and SAED patterns (Fig. 5b) also showed that the GR_{SO4} particles in the 90-day long interacted samples maintained their well-defined thin hexagonal plate-like morphology and crystal structure. These observations were also confirmed by the fact that the long-term monitoring of aqueous As in the supernatant (Fig. S6) revealed that the initial adsorbed As was not released back into the aqueous phase. Previous studies have shown that adsorbed As can slow down or inhibit the transformation of GR minerals to other iron (oxyhydr)oxides such as magnetite (Su and Wilkin, 2005; Wang et al., 2014), which explains the stability of the As-interacted GR_{SO4} even after 90 days in our study. In addition, our results are also consistent with long-term batch experiments of Su and Wilkin (2005), who showed that As-interacted GR_{CO3} remained stable for up to 60 days.

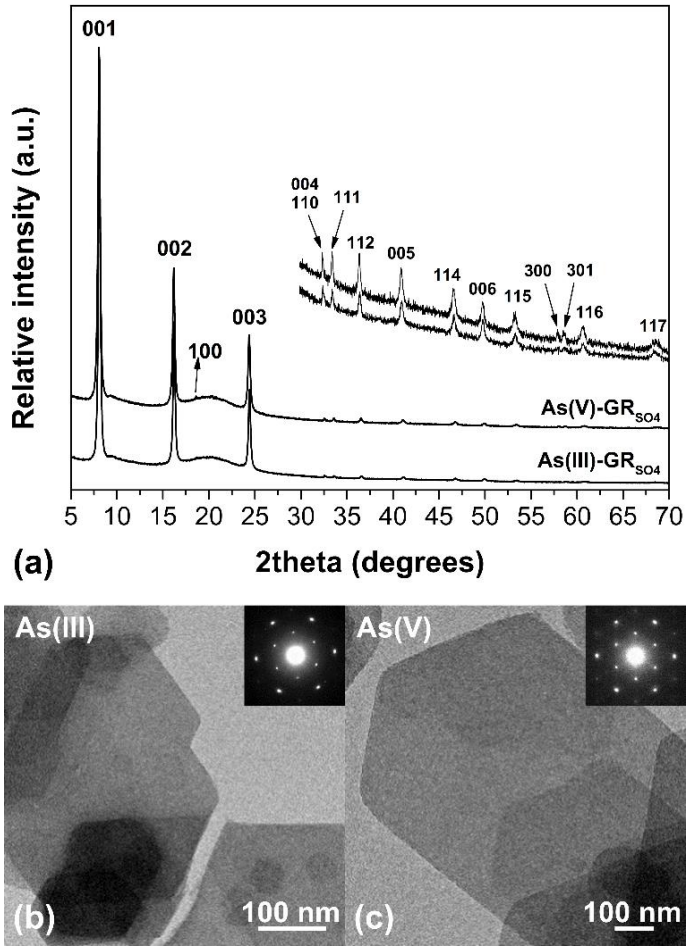

Fig. 5. (a) XRD patterns and (b-c) TEM images (inset: SAED pattern) GR_{SO4} interacted with 10 mg L^{-1} As(III) and As(V) after 90 days. XRD peaks of GR_{SO4} were assigned based on published diffraction data (Simon et al., 2003). The broad amorphous hump at ~20° 2θ comes from the XRD sample holder.

3.5 Adsorption isotherms and mechanism

The As adsorption isotherms at all tested pH values are shown in Fig. 6. Equilibrium adsorption data were fitted to Langmuir and Freundlich isotherm models and the calculated fitting parameters for both models are shown in Table S7. Based on the fitting, the adsorption of As species on GR_{SO4} is best described using the Langmuir model, indicating a homogenous monolayer binding of As surface complexes at the solid/water interface (Leus et al., 2017). Using the Langmuir adsorption model, we determined the maximum As adsorption capacities for both As species onto GR_{SO4} (Table 1). At alkaline pH, the maximum adsorption capacity of As(III) was 2.2 times higher than the value at

neutral pH, while As(V) had 1.5 times higher maximum adsorption capacity at pH 7 compared to pH 8-9.

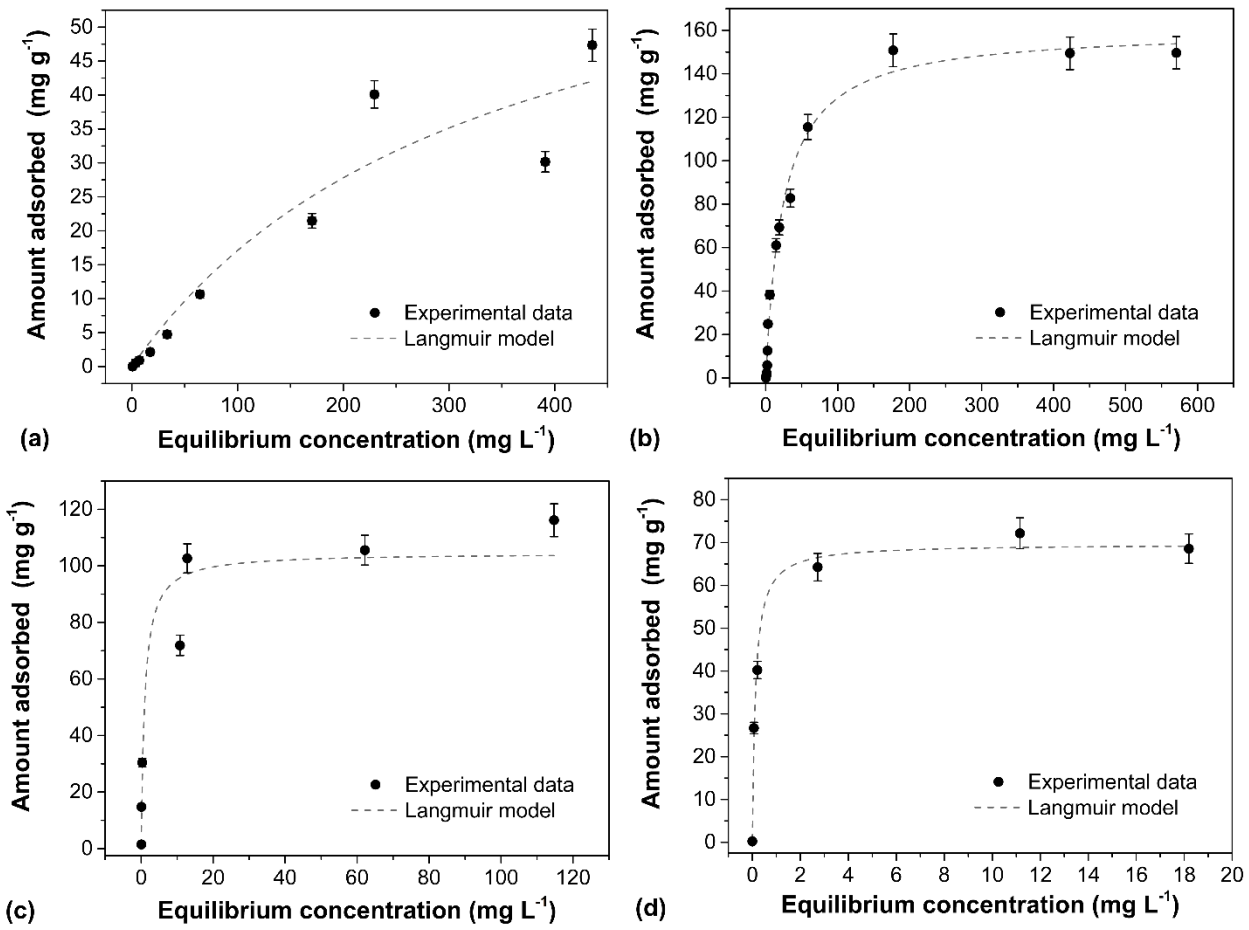

Fig. 6. Langmuir adsorption isotherms of As species on GR_{SO4}. (a-b) Adsorption of As(III) at pH 7 and 8-9, respectively. (c-d) Adsorption of As(V) at pH 7 and 8-9, respectively. Error bars represent analytical uncertainty (< 5% relative) based on replicate measurements of QC solutions analyzed together with the samples (Table S1).

The spatial distribution of the adsorbed As(III) on the GR particles, at an initial concentration of 500 mg L^{-1}, was examined using HAADF-STEM imaging coupled with EDX mapping (Fig. 7). The EDX elemental map (Fig. 7d) and associated intensity profile (Fig. 7g) show higher concentrations of As can be found near the GR particle edges (*ca.* two times higher than the 001 GR surface). In addition, the HAADF-STEM image (Fig. 7a) alone shows increased intensity at the GR

particle edges which we interpret to be associated with increased As concentration. These results, combined with the adsorption isotherm results, strengthen previous findings that suggested that As(III) and As(V) form monodentate mononuclear (^1V) and bidentate binuclear (^2C) inner-sphere complexes on the GR particle edges (Jönsson and Sherman, 2008; Wang et al., 2010). However, the maximum adsorption capacity for As(III) determined in the current study could also indicate that surface complexation may not be limited to the GR_{SO4} particle edges but, as mentioned before, may also result from the presence of multi-nuclear arsenite complexes (Ona-Nguema et al., 2009; Wang et al., 2010).

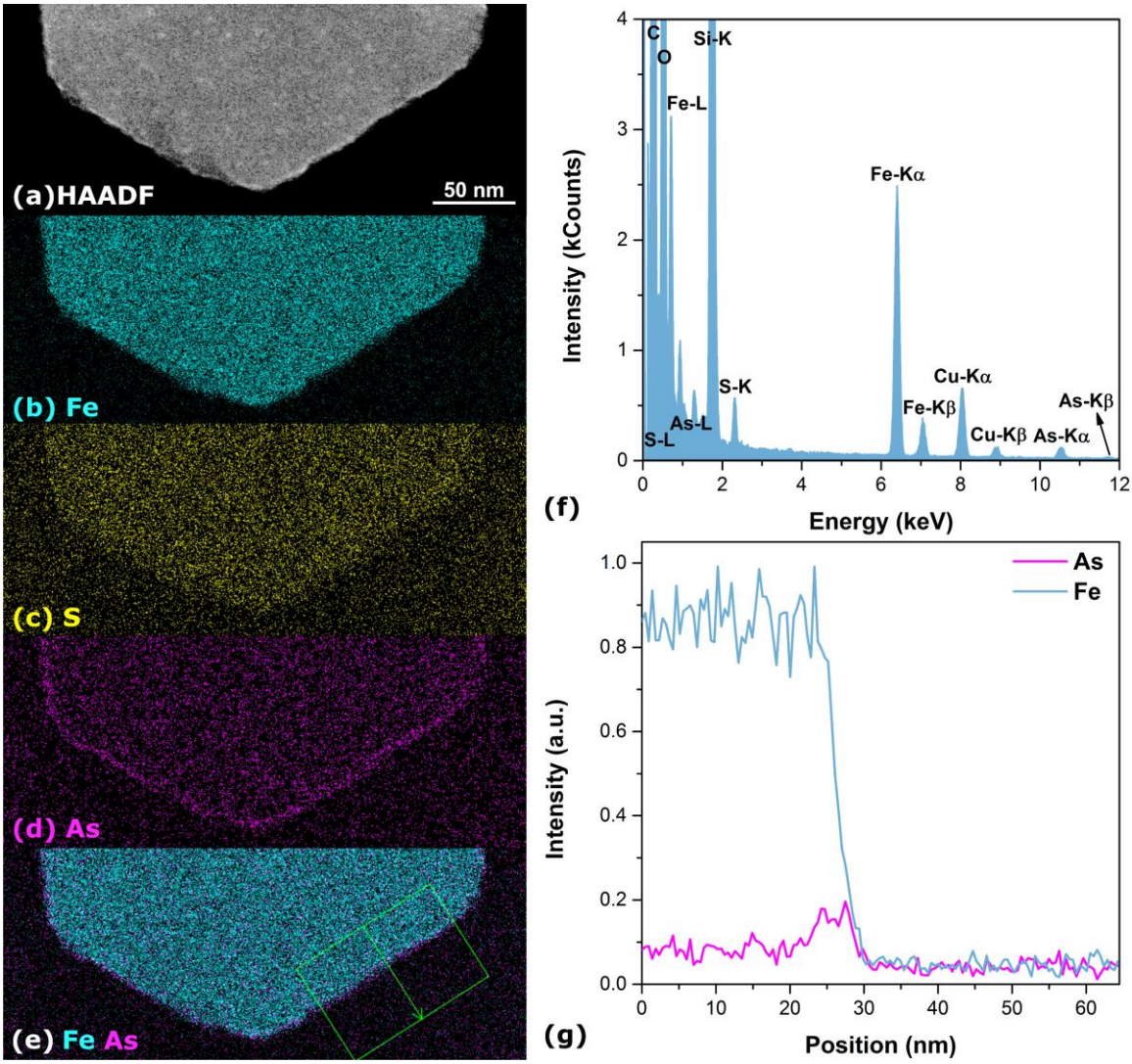

Fig. 7. (a) HAADF-STEM overview of GR_{SO4} interacted with 500 mg L^{-1} of As(III) and the corresponding (b) EDX elemental maps for (b) Fe (light blue), (c) S (yellow), (d) As (magenta) and

(e) combined Fe and As. (f) The EDX spectrum of (a). The Si signal comes from the use of headspace crimp vials while C and Cu peaks come from the TEM grid. (g) The EDX signal intensity profile shows the change in concentration of Fe and As along the integrated line drawn across the marked area in green (e).

In addition to surface complexation, previous studies with selenate have shown that tetrahedral oxyanions (e.g., SeO_4^{2-}) can also be removed by GR phases by interlayer intercalation (Refait et al., 2000). In our study intercalation of As(III) and As(V) in the interlayer region of GR would have resulted in changes in the basal spacing since the ionic radius of AsO_3^{3-} (2.11 Å) and AsO_4^{3-} (2.48 Å) are different to that of SO_4^{2-} (2.30 Å) (Goh et al., 2008). However, XRD patterns of GR_{SO4} interacted with As(III) and As(V) at 10 mg L^{-1} (Fig. 5a) and 500 mg L^{-1} (Fig. S7) did not exhibit shifts in the basal (001) reflections (~10.93 Å) to accommodate such intercalations. The intercalation of As(III) and As(V) in our study, might have been inhibited because SO_4^{2-} cannot be readily exchanged in layered double hydroxides (de Roy et al., 2001; Miyata, 1983).

3.6 Environmental significance of GR minerals in As-contaminated environments

Using the adsorption isotherm modelling data, we compared the calculated adsorption capacities for As species on GR_{SO4} and with literature data for all described iron (oxyhydr)oxides, oxyhydroxysulfates and sulfides, which have also been evaluated for their efficiency as mineral substrate for the treatment of As contaminated groundwater resources (Table 1).

Our data show clearly that GR_{SO4} is among the most effective adsorbents among all the phases listed in Table 1. This finding has important implications for the fate and mobility of As in anoxic groundwaters where GR_{SO4} exists. To the best of our knowledge, this is the first study to report the adsorption isotherms of As(III) and As(V) for GR_{SO4}, as well as the in-depth examination of critical adsorption parameters for As removal. We have shown that at circum-neutral and slightly alkaline pH conditions, GR_{SO4} can efficiently adsorb large amounts of As(III) and As(V), making GR_{SO4} one of the best performing iron-bearing mineral phases in terms of As adsorption. For As(III) at slightly alkaline pH, GR_{SO4} is only outperformed by ferrihydrite (Table 1 entry 5) and

schwertmannite (Table 1 entry 6) (Davidson et al., 2008). Ferrihydrite and schwertmannite are poorly ordered, highly reactive and thermodynamically metastable iron-bearing mineral phases which can transform at ambient conditions to more thermodynamically stable crystalline iron (oxyhydr)oxides such as goethite and hematite, fast at alkaline conditions but slow at near-neutral pH values (Brinza et al., 2015; Burton et al., 2008; Davidson et al., 2008; Vu et al., 2013; Yee et al., 2006). Moreover, comparing our data with other Fe-bearing phases (Table 1) shows thatamong mixed-valent and redox-active iron (oxyhydr)oxides and sulphides, GR_{SO4} exhibits an unprecedented As(III) uptake and also remains stable for long time periods. Even compared to magnetite (Table 1 entry 4) and iron sulfides (e.g., troilite, pyrite; Table 1 entries 7-9) that are crystalline and highly stable in reduced environments, our GR_{SO4} showed higher adsorption capacities. This exceptional As adsorption capacity makes GR_{SO4} a novel and potentially highly environmentally-relevant mineral substrate for As sequestration in near-neutral pH and reduced to slightly oxidized groundwater systems.

Table 1. Comparison of As adsorption capacities of GR_{SO4} with common iron (oxyhydr)oxides, oxyhydroxysulfates and sulfides.

Entry No.	Adsorbent	Particle size (nm)	Surface area (m^2 g^{-1})[a]	Tested pH	Adsorption capacity (mg g^{-1}) As(III)	As(V)	Reference
1	Goethite	-	39	9	22.0	4.0	Lenoble et al. (2002)
2	Hematite	5	162	7	95.0	47.0	Tang et al. (2011)
3	Maghemite	7-12	169	-	67.0	95.4	Lin et al. (2012)
4	Magnetite	12	99	8	134.9	172.3	Yean et al. (2005)
5	Ferrihydrite	-	202	5	552.9	222.1	Raven et al. (1998)
6	Schwertmannite	-	280[b]	9	280.4	166.5	Burton et al. (2009)
7	Mackinawite	2	350	7	9.7	32.2	Wolthers et al. (2005)
8	Troilite	-	3	7	17.3	-	Bostick and Fendorf (2003)
9	Pyrite	-	41	7	1.0	-	Bostick and Fendorf (2003)
10	GR_{CO3}	100-300	-	7.5	123.0	-	Su & Wilkin (2005)
11	GR_{SO4}	50-500	- 25[c]	10.5 7 8-9	43.8 74.0 160.3	6.91 104.5 69.6	Su & Wilkin (2005) This work This work

[a] Specific surface area determined by the Brunauer–Emmett–Teller (BET) model. [b] Estimated from Davidson et al. (2008) [c] Measured nitrogen sorption isotherm can be found in Fig. S5.

Previous studies have shown that GR phases can oxidize As(III) to As(V) (Su and Puls, 2004; Su and Wilkin, 2005). Although not investigated in this study, possible redox transformation can heavily impact the toxicity and mobility of As in soils and groundwaters. As(III) oxidation by GR mineral phases would be a favorable process as it would result in a less toxic and less mobile As(V) species (Vaughan, 2006). On the other hand, reduction of As(V) to the far more toxic As(III) and the potential re-release into groundwaters because of the lower affinity of As(III) for ferric iron (oxyhydr)oxides would be far more damaging (Roberts et al., 2004). Further studies are needed to confirm the potential of As(III) oxidation in the presence of GR and to determine the geochemical and thermodynamic driving forces in this reaction.

As for redox-active mineral adsorbents, arsenic can still be released from GR_{SO4} since its sequestration is highly dependent on pH conditions and redox environment. Sudden changes in pH or Eh of the system may cause potential release of surface immobilized As species back into the groundwater either by dissolution or redox-change driven transformation of GR phases (Cundy et al., 2008). Iron mineral phases such as goethite and magnetite, which are common transformation end-products of GR, are, however, far less reactive and effective mineral substrates for As sequestration (Table 1), which can lead to remobilization of As in groundwaters.

4. Conclusions

In this work, we investigated the interfacial reactivity between GR_{SO4} and As species. An extensive batch adsorption study was performed to examine the influence of various critical environmental parameters such as initial concentration, pH, adsorbent loading, ionic strength and presence of potentially interfering ions on As removal. We have successfully demonstrated that GR_{SO4} is an effective and stable As(III) and As(V) mineral adsorbent compared to other iron (oxyhydr)oxide phases. GR_{SO4} demonstrated remarkable maximum adsorption capacities for As(III) and As(V) of up to 160 and 105 mg g^{-1}, respectively. This exceptional As adsorption reactivity makes GR a potentially

novel and environmentally-relevant mineral substrate for the sequestration of As in reduced groundwater systems. The removal of As is also highly pH dependent – high As(III) removal was obtained at higher pH while As(V) removal was found to be more favourable at circum-neutral conditions. GR_{SO4} exhibited fast As uptake rates at alkaline conditions. Common groundwater species such as Mg^{2+} and PO_4^{3-} were found to affect the efficiency of As adsorption onto GR_{SO4}. Overall, our results clearly highlight importance of redox-active GR mineral phases in removing As species from aqueous solutions and their potential crucial role in the remediation of contaminated groundwaters.

Acknowledgement

This project has received funding from the European Union's Horizon 2020 Marie Sklodowska-Curie Innovative Training Network Grant No. 675219 for JPHP and LGB and the German Helmholtz Recruiting Initiative funding to LGB and HMF. ICP-OES analyses were carried out at the Helmholtz Laboratory for the Geochemistry of the Earth Surface (HELGES), GFZ Potsdam. We thank Rogier Besselink from the Interface Geochemistry Section at GFZ for the help with the BET analyses; Andrea Vieth-Hillebrand from the Organic Geochemistry Section at GFZ for the help with ion chromatography analysis; and Andy Brown from the Leeds Electron Microscopy and Spectroscopy Centre (LEMAS), University of Leeds, for the help with electron diffraction and EDX mapping, and for providing reference EEL spectra for hedenbergite and hematite samples. We also acknowledge the help of Jörg Radnik from the German Federal Institute for Materials Research and Testing (BAM) with the XPS analyses and of Peter Adler from the Max Planck Institute for Chemical Physics of Solids for the Mössbauer analysis. XRD analyses were done with the assistance of Marco Mangayayam and Dominique J. Tobler from NanoGeoScience, University of Copenhagen. The authors would also like to thank Robin Wojcik of the Interface Geochemistry Section at GFZ for his help in the graphical abstract.

Appendix A. Supplementary data

Details on mineral characterization and data (XRD, TEM, SAED, EDX, EELS, N_2 sorption, XPS, Mössbauer spectroscopy, ICP-OES, ion chromatography), batch adsorption experimental

methods and data and aqueous concentration analysis of long-term batch experiments can be found in the Supporting Information. Supplementary data associated with this article can be found in the online version.

References

Ahmed IAM, Benning LG, Kakonyi G, Sumoondur AD, Terrill NJ, Shaw S. Formation of green rust sulfate: A combined *in situ* time-resolved X-ray scattering and electrochemical study. Langmuir 2010; 26: 6593-6603.

Ahmed IAM, Shaw S, Benning LG. Formation of hydroxysulphate and hydroxycarbonate green rusts in the presence of zinc using time-resolved *in situ* small and wide angle X-ray scattering. Mineralogical Magazine 2008; 72: 159-162.

Asere TG, De Clercq J, Verbeken K, Tessema DA, Fufa F, Stevens CV, Du Laing G. Uptake of arsenate by aluminum (hydr)oxide coated red scoria and pumice. Applied Geochemistry 2017; 78: 83-95.

Bocher F, Géhin A, Ruby C, Ghanbaja J, Abdelmoula M, Génin J-MR. Coprecipitation of Fe(II–III) hydroxycarbonate green rust stabilised by phosphate adsorption. Solid State Sciences 2004; 6: 117-124.

Bostick BC, Fendorf S. Arsenite sorption on troilite (FeS) and pyrite (FeS_2). Geochimica et Cosmochimica Acta 2003; 67: 909-921.

Brinza L, Vu HP, Shaw S, Mosselmans JFW, Benning LG. Effect of Mo and V on the hydrothermal crystallization of hematite from ferrihydrite: An *in situ* energy dispersive X-ray diffraction and X-ray absorption spectroscopy study. Crystal Growth & Design 2015; 15: 4768-4780.

Brown AP, Hillier S, Brydson RMD. Quantification of Fe-oxidation state in mixed valence minerals: a geochemical application of EELS revisited. Journal of Physics: Conference Series 2017; 902: 012016.

Burton ED, Bush RT, Johnston SG, Watling KM, Hocking RK, Sullivan LA, Parker GK. Sorption of arsenic(V) and arsenic(III) to schwertmannite. Environmental Science & Technology 2009; 43: 9202-9207.

Burton ED, Bush RT, Sullivan LA, Mitchell DRG. Schwertmannite transformation to goethite via the Fe(II) pathway: Reaction rates and implications for iron–sulfide formation. Geochimica et Cosmochimica Acta 2008; 72: 4551-4564.

Christiansen BC, Balic-Zunic T, Petit PO, Frandsen C, Mørup S, Geckeis H, Katerinopoulou A, Stipp SLS. Composition and structure of an iron-bearing, layered double hydroxide (LDH) – Green rust sodium sulphate. Geochimica et Cosmochimica Acta 2009; 73: 3579-3592.

Christiansen BC, Geckeis H, Marquardt CM, Bauer A, Römer J, Wiss T, Schild D, Stipp SLS. Neptunyl (Np) interaction with green rust. Geochimica et Cosmochimica Acta 2011; 75: 1216-1226.

Cundy AB, Hopkinson L, Whitby RLD. Use of iron-based technologies in contaminated land and groundwater remediation: A review. Science of The Total Environment 2008; 400: 42-51.

Davidson LE, Shaw S, Benning LG. The kinetics and mechanisms of schwertmannite transformation to goethite and hematite under alkaline conditions. American Mineralogist 2008; 93: 1326.

de Roy A, Forano C, Besse JP. Layered Double Hydroxides: Synthesis and Post-Synthesis Modification. In: Rives V, editor. Layered Double Hydroxides: Present and Future. Nova Science Publishers, New York, 2001, pp. 1-39.

Ferguson JF, Gavis J. A review of the arsenic cycle in natural waters. Water Research 1972; 6: 1259-1274.

Folens K, Leus K, Nicomel NR, Meledina M, Turner S, Van Tendeloo G, Laing GD, Van Der Voort P. Fe_3O_4@MIL-101 - A selective and regenerable adsorbent for the removal of As species from water. European Journal of Inorganic Chemistry 2016: 4395-4401.

512 Géhin A, Ruby C, Abdelmoula M, Benali O, Ghanbaja J, Refait P, Génin J-MR. Synthesis of Fe(II-
513 III) hydroxysulphate green rust by coprecipitation. Solid State Sciences 2002; 4: 61-66.
514 Génin J-MR, Ruby C. Anion and cation distributions in Fe(II–III) hydroxysalt green rusts from XRD
515 and Mössbauer analysis (carbonate, chloride, sulphate, …); the "fougerite" mineral. Solid State
516 Sciences 2004; 6: 705-718.
517 Goh K-H, Lim T-T, Dong Z. Application of layered double hydroxides for removal of oxyanions: A
518 review. Water Research 2008; 42: 1343-1368.
519 Guilbaud R, White ML, Poulton SW. Surface charge and growth of sulphate and carbonate green rust
520 in aqueous media. Geochimica et Cosmochimica Acta 2013; 108: 141-153.
521 Guo X, Chen F. Removal of Arsenic by Bead Cellulose Loaded with Iron Oxyhydroxide from
522 Groundwater. Environmental Science & Technology 2005; 39: 6808-6818.
523 Gupta A, Chauhan VS, Sankararamakrishnan N. Preparation and evaluation of iron–chitosan
524 composites for removal of As(III) and As(V) from arsenic contaminated real life groundwater.
525 Water Research 2009; 43: 3862-3870.
526 Ho Y-S. Review of second-order models for adsorption systems. Journal of Hazardous Materials
527 2006; 136: 681-689.
528 Hongshao Z, Stanforth R. Competitive adsorption of phosphate and arsenate on goethite.
529 Environmental Science & Technology 2001; 35: 4753-4757.
530 Hughes MF. Arsenic toxicity and potential mechanisms of action. Toxicology Letters 2002; 133: 1-
531 16.
532 Inskeep WP, McDermott TR, Fendorf S. Arsenic (V)/(III) recycling in soils and natural waters:
533 Chemical and microbiological processes. In: Frankenberger WT, editor. Environmental
534 Chemistry of Arsenic. Marcel Dekker, New York, 2002, pp. 183-215.
535 Jain A, Raven KP, Loeppert RH. Arsenite and Arsenate Adsorption on Ferrihydrite: Surface Charge
536 Reduction and Net OH- Release Stoichiometry. Environmental Science & Technology 1999;
537 33: 1179-1184.
538 Jönsson J, Sherman DM. Sorption of As(III) and As(V) to siderite, green rust (fougerite) and
539 magnetite: Implications for arsenic release in anoxic groundwaters. Chemical Geology 2008;
540 255: 173-181.
541 Lenoble V, Bouras O, Deluchat V, Serpaud B, Bollinger J-C. Arsenic adsorption onto pillared clays
542 and iron oxides. Journal of Colloid and Interface Science 2002; 255: 52-58.
543 Leus K, Folens K, Nicomel NR, Perez JPH, Filippousi M, Meledina M, Dîrtu MM, Turner S, Van
544 Tendeloo G, Garcia Y, Du Laing G, Van Der Voort P. Removal of arsenic and mercury species
545 from water by covalent triazine framework encapsulated γ-Fe_2O_3 nanoparticles. Journal of
546 Hazardous Materials 2018; 353: 312-319.
547 Leus K, Perez JPH, Folens K, Meledina M, Van Tendeloo G, Du Laing G, Van Der Voort P. UiO-66-
548 $(SH)_2$ as stable, selective and regenerable adsorbent for the removal of mercury from water
549 under environmentally-relevant conditions. Faraday Discussions 2017; 201: 145-161.
550 Lightstone FC, Schwegler E, Hood RQ, Gygi F, Galli G. A first principles molecular dynamics
551 simulation of the hydrated magnesium ion. Chemical Physics Letters 2001; 343: 549-555.
552 Limousin G, Gaudet JP, Charlet L, Szenknect S, Barthès V, Krimissa M. Sorption isotherms: A
553 review on physical bases, modeling and measurement. Applied Geochemistry 2007; 22: 249-
554 275.
555 Lin S, Lu D, Liu Z. Removal of arsenic contaminants with magnetic γ-Fe_2O_3 nanoparticles. Chemical
556 Engineering Journal 2012; 211–212: 46-52.
557 Malis T, Cheng SC, Egerton RF. EELS log-ratio technique for specimen-thickness measurement in
558 the TEM. Journal of Electron Microscopy Technique 1988; 8: 193-200.
559 Masscheleyn PH, Delaune RD, Patrick WH. Arsenic and selenium chemistry as affected by sediment
560 redox potential and pH. Journal of Environmental Quality 1991; 20: 522-527.
561 Mitsunobu S, Takahashi Y, Sakai Y, Inumaru K. Interaction of synthetic sulfate green rust with
562 antimony(V). Environmental Science & Technology 2009; 43: 318-323.
563 Miyata S. Anion-exchange properties of hydrotalcite-like compounds. Clays Clay Miner 1983; 31:
564 305-311.

565 Mullet M, Guillemin Y, Ruby C. Oxidation and deprotonation of synthetic Fe^{II}-Fe^{III}
566 (oxy)hydroxycarbonate Green Rust: An X-ray photoelectron study. Journal of Solid State
567 Chemistry 2008; 181: 81-89.
568 Nedel S, Dideriksen K, Christiansen BC, Bovet N, Stipp SLS. Uptake and release of cerium during
569 Fe-oxide formation and transformation in Fe(II) solutions. Environmental Science &
570 Technology 2010; 44: 4493-4498.
571 Nickson RT, McArthur JM, Ravenscroft P, Burgess WG, Ahmed KM. Mechanism of arsenic release
572 to groundwater, Bangladesh and West Bengal. Applied Geochemistry 2000; 15: 403-413.
573 O'Loughlin EJ, Kelly SD, Cook RE, Csencsits R, Kemner KM. Reduction of uranium(VI) by mixed
574 iron(II)/iron(III) hydroxide (green rust): Formation of UO_2 nanoparticles. Environmental
575 Science & Technology 2003; 37: 721-727.
576 Ona-Nguema G, Morin G, Wang Y, Menguy N, Juillot F, Olivi L, Aquilanti G, Abdelmoula M, Ruby
577 C, Bargar JR, Guyot F, Calas G, Brown GE. Arsenite sequestration at the surface of nano-
578 $Fe(OH)_2$, ferrous-carbonate hydroxide, and green-rust after bioreduction of arsenic-sorbed
579 lepidocrocite by *Shewanella putrefaciens*. Geochimica et Cosmochimica Acta 2009; 73: 1359-
580 1381.
581 Randall SR, Sherman DM, Ragnarsdottir KV. Sorption of As(V) on green rust
582 ($Fe_4(II)Fe_2(III)(OH)_{12}SO_4 \cdot 3H_2O$) and lepidocrocite (γ-FeOOH): Surface complexes from
583 EXAFS spectroscopy. Geochimica et Cosmochimica Acta 2001; 65: 1015-1023.
584 Raven KP, Jain A, Loeppert RH. Arsenite and arsenate adsorption on ferrihydrite: Kinetics,
585 equilibrium, and adsorption envelopes. Environmental Science & Technology 1998; 32: 344-
586 349.
587 Refait P, Bauer P, Olowe AA, Genin JMR. The substitution of Fe^{2+} ions by Ni^{2+} ions in the green rust
588 2 compound studied by Mössbauer effect. Hyperfine Interactions 1990; 57: 2061-2066.
589 Refait P, Simon L, Génin J-MR. Reduction of SeO_4^{2-} anions and anoxic formation of iron(II)−iron(III)
590 hydroxy-selenate green rust. Environmental Science & Technology 2000; 34: 819-825.
591 Roberts LC, Hug SJ, Ruettimann T, Billah MM, Khan AW, Rahman MT. Arsenic removal with
592 iron(II) and iron(III) in waters with high silicate and phosphate concentrations. Environmental
593 Science & Technology 2004; 38: 307-315.
594 Schuessler JA, Kämpf H, Koch U, Alawi M. Earthquake impact on iron isotope signatures recorded in
595 mineral spring water. Journal of Geophysical Research: Solid Earth 2016; 121: 8548-8568.
596 Sharma VK, Sohn M. Aquatic arsenic: Toxicity, speciation, transformations, and remediation.
597 Environment International 2009; 35: 743-759.
598 Shipley HJ, Yean S, Kan AT, Tomson MB. Adsorption of arsenic to magnetite nanoparticles: Effect
599 of particle concentration, pH, ionic strength, and temperature. Environmental Toxicology and
600 Chemistry 2009; 28: 509-515.
601 Simon L, François M, Refait P, Renaudin G, Lelaurain M, Génin J-MR. Structure of the Fe(II-III)
602 layered double hydroxysulphate green rust two from Rietveld analysis. Solid State Sciences
603 2003; 5: 327-334.
604 Skovbjerg LL, Stipp SLS, Utsunomiya S, Ewing RC. The mechanisms of reduction of hexavalent
605 chromium by green rust sodium sulphate: Formation of Cr-goethite. Geochimica et
606 Cosmochimica Acta 2006; 70: 3582-3592.
607 Smedley PL, Kinniburgh DG. A review of the source, behaviour and distribution of arsenic in natural
608 waters. Applied Geochemistry 2002; 17: 517-568.
609 Su C, Puls RW. Significance of iron(II,III) hydroxycarbonate green rust in arsenic remediation using
610 zerovalent iron in laboratory column tests. Environmental Science & Technology 2004; 38:
611 5224-5231.
612 Su C, Wilkin RT. Arsenate and arsenite sorption on and arsenite oxidation by iron(II, III)
613 hydroxycarbonate green rust. Advances in Arsenic Research. 915. American Chemical Society,
614 2005, pp. 25-40.
615 Tang W, Li Q, Gao S, Shang JK. Arsenic (III,V) removal from aqueous solution by ultrafine α-Fe_2O_3
616 nanoparticles synthesized from solvent thermal method. Journal of Hazardous Materials 2011;
617 192: 131-138.

618 Usman M, Byrne JM, Chaudhary A, Orsetti S, Hanna K, Ruby C, Kappler A, Haderlein SB.
619 Magnetite and green rust: Synthesis, properties, and environmental applications of mixed-
620 valent iron minerals. Chemical Reviews 2018; 118: 3251-3304.
621 Vaughan DJ. Arsenic. Elements 2006; 2: 71-75.
622 Vu HP, Shaw S, Brinza L, Benning LG. Partitioning of Pb(II) during goethite and hematite
623 crystallization: Implications for Pb transport in natural systems. Applied Geochemistry 2013;
624 39: 119-128.
625 Wang Y, Morin G, Ona-Nguema G, Brown GE. Arsenic(III) and arsenic(V) speciation during
626 transformation of lepidocrocite to magnetite. Environmental Science & Technology 2014; 48:
627 14282-14290.
628 Wang Y, Morin G, Ona-Nguema G, Juillot F, Guyot F, Calas G, Brown GE. Evidence for different
629 surface speciation of arsenite and arsenate on green rust: An EXAFS and XANES Study.
630 Environmental Science & Technology 2010; 44: 109-115.
631 Williams M, Fordyce F, Paijitprapapon A, Charoenchaisri P. Arsenic contamination in surface
632 drainage and groundwater in part of the southeast Asian tin belt, Nakhon Si Thammarat
633 Province, southern Thailand. Environmental Geology 1996; 27: 16-33.
634 Wolthers M, Charlet L, van Der Weijden CH, van der Linde PR, Rickard D. Arsenic mobility in the
635 ambient sulfidic environment: Sorption of arsenic(V) and arsenic(III) onto disordered
636 mackinawite. Geochimica et Cosmochimica Acta 2005; 69: 3483-3492.
637 World Health Organization. Guidelines for drinking-water quality: Fourth edition incorporating the
638 first addendum. Geneva, 2017.
639 Yean S, Cong L, Yavuz CT, Mayo JT, Yu WW, Kan AT, Colvin VL, Tomson MB. Effect of
640 magnetite particle size on adsorption and desorption of arsenite and arsenate. Journal of
641 Materials Research 2005; 20: 3255-3264.
642 Yee N, Shaw S, Benning LG, Nguyen TH. The rate of ferrihydrite transformation to goethite via the
643 Fe(II) pathway. American Mineralogist 2006; 91: 92-96.
644 Zahid A, Hassan MQ, Balke KD, Flegr M, Clark DW. Groundwater chemistry and occurrence of
645 arsenic in the Meghna floodplain aquifer, southeastern Bangladesh. Environmental Geology
646 2008; 54: 1247-1260.